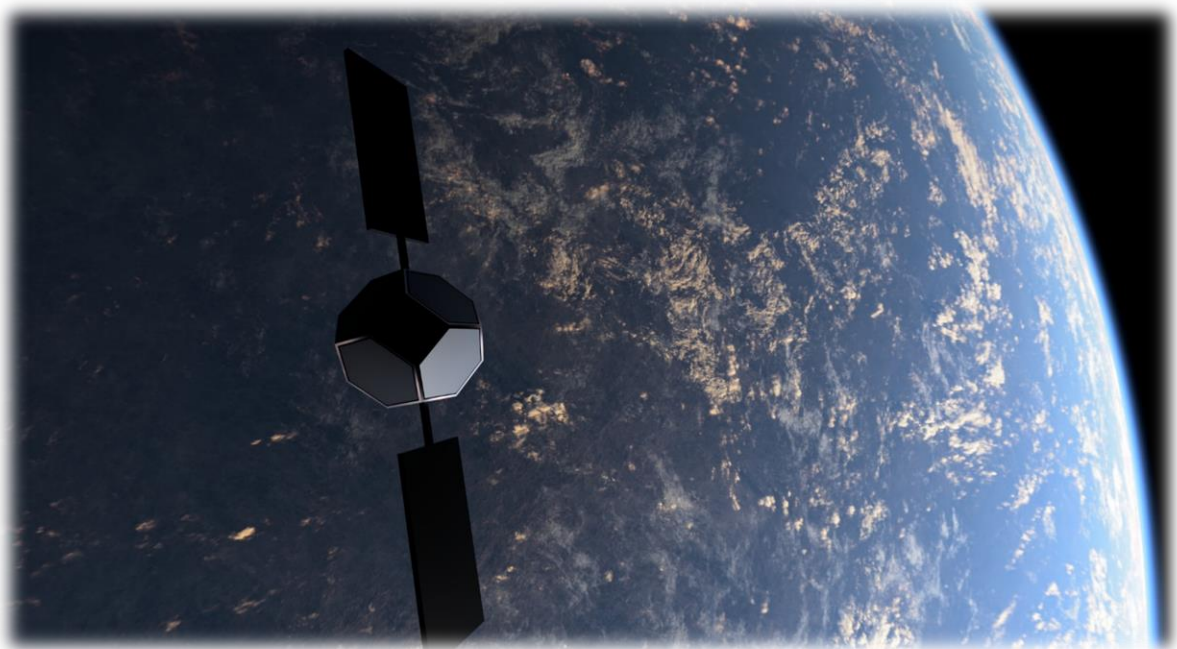




PLANETARY DEORBITER FOR ACTIVE SPACE DEBRIS REMOVAL – PETER-1

Final Year Project Report




IONUT IONITA
UNIVERSITY OF CENTRAL LANCASHIRE

Submitted in partial satisfaction of the
requirements for the degree of

Bachelor of Engineering (with Honours)
in
Robotics Engineering
March 2023

I declare that all material contained in
this report, including ideas described in
the text, computer programs and
drawings, is my own work except where
explicitly and individually
acknowledged.

Signed 

Date: 31st Of March 2023

Acknowledgements

Foremost, I would like to express the deepest appreciation and gratitude to my supervisor Stephen Sigurnjak and my moderator Carl Berry for their continuous support of my project, for their patience, enthusiasm and expertise throughout my research.

I would like to like to extend gratitude to Mara Bernabei for her support during my degree, her motivation and dedication played a significant role in shaping my academic progress.

I am deeply grateful to family and my fiancée Madalina Avram. Whose love, encouragement, sacrifices and understanding have been the driving force behind my success and helped me overcome the challenges of encountered during my degree.

Thank you.

Dedication

This project is dedicated to my grandfather.

Peter

Miss you

Table of Contents

Chapter 1: Introduction and Motivation.....	6
1.1 Space Debris.....	6
1.2 Space Debris Population and Sustainability.....	7
1.3 PETER-1 Mission Concept	9
Chapter 2: Literature Review	10
2.1 Mitigation, Remediation and On-Orbit Servicing.....	10
2.2 Computer Vision and Deep Learning	12
2.2.1 Stereo Vision and Depth Estimation	13
Chapter 3: Methodology.....	15
3.1 System Components	15
3.2 System Implementation Diagram	17
.....	17
3.3 Object Detection	18
3.3.1 Dataset Preparation and Training.....	19
.....	20
3.4 Design Evolution and Manufacturing	21
Chapter 4: Testing and Results	23
4.1 YOLO Model Results.....	23
4.2 Module implementation	24
Chapter 5: Conclusion and further development	26

List of Figures

Figure 1 NASA-LEGEND catalogue of objects > 10cm in LEO (credits NASA ODPO)	7
Figure 2 Mission Concept.....	9
Figure 3: Number of cumulative collisions and number of objects in LEO in the simulated scenarios of long-term evolution of the environment, ESA 2022.....	10
Figure 4 Stereo vision.....	13
Figure 5 Epipolar Geometry	13
Figure 6 Image formation using a stereo camera	14
Figure 7 System Implementation.....	17
Figure 8 Comparison between SSD and MSD models	18
Figure 9 Simulated Space Debris Object	19
Figure 10 YOLO label format.....	19
Figure 11 Labelled Dataset.....	20
Figure 12 Results from the YOLO traing on GoogleColab	23
Figure 13 Module Simulation.....	24
Figure 14 Belt Tensioner	25
Figure 15 Object detected using the OAK-D camera	25

Chapter 1: Introduction and Motivation

1.1 Space Debris

The era of space exploration has begun with the launch of the first satellite into space in 1957, the Sputnik-1. However, the concept of launching a man-made object to space have been discredited for many years before Sputnik-1 as the general views at the time could not find a real necessity to send an object to space. The feasibility of using reactive force to send a vehicle into space has been mathematically proven by the Russian scientist Konstantin Tsiolkovskiy in 1903, who worked alongside other pioneers such as the Romanian-born physicist Hermann Oberth (Constance McLaughlin Green, et. al 1970)

In over half a century, space activities have grown exponentially specially in the last decades with the introduction of artificial constellations made of telecommunication satellites. Although the development of the satellite industry shaped our lives, the proliferation of space debris is a growing concern for the international space community as it has started to endanger human missions including the International Space Station (ISS) and the SpaceX Crew Dragon missions (NASA, 2021). Furthermore, space debris represent a severe threat to functional satellites orbiting Earth as there is a continuously growing risk of collisions where satellites must perform complex collision avoidance manoeuvres consuming valuable fuel resources therefore reducing their operational life.

The type of orbit for a satellite is selected based on its usage, for instance telecommunications satellites must stay 'stationary' above a certain point over Earth therefore are located within the Geostationary orbit (GEO), a circular orbit above the equator that follows the Earth's rotation from west to east making each point on the orbit to correspond to a specific point on Earth. However, the predominant orbit used is the Low Earth orbit (LEO) because of its low altitude spreading between 200 km to 2000 km, the satellites within this orbit do not have to follow the same path around Earth but their plane can be tilted, increasing the available routes that they travel. The proximity to Earth's surface makes LEO to be used by the International Space Station (ISS), it also means that the satellites can complete an orbit in approximately 90 minutes. Due to the high-speed LEO is not suitable for telecommunications satellites, however they can be implemented into a net called artificial constellation. In the last decades the number of satellites in LEO have increased exponentially with the expansion of artificial constellations but also the high number of CubeSats (harder to track and monitor due their small dimensions), making the orbit become densely populated, because of the speed of these objects' collisions have started to increment excessively creating a high number of space debris (ESA, 2020).

1.2 Space Debris Population and Sustainability

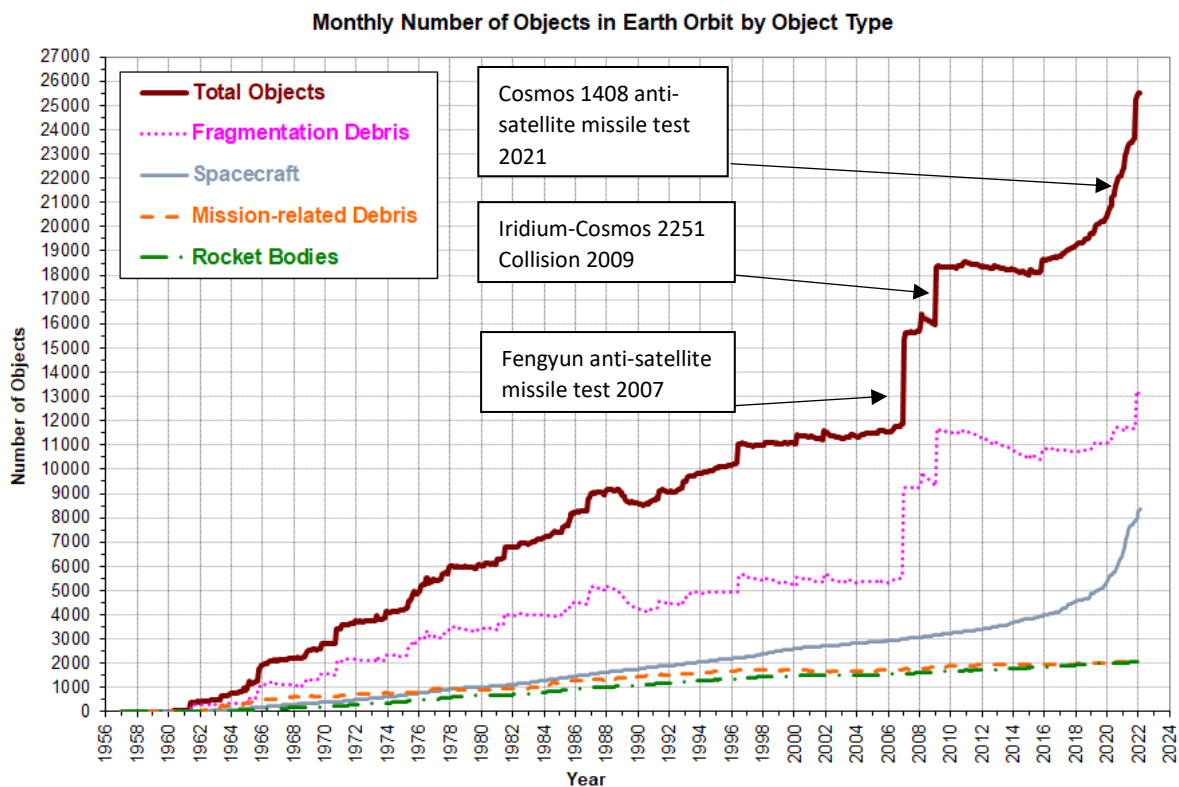


Figure 1 NASA-LEGEND catalogue of objects > 10cm in LEO (credits NASA ODPO)

According to the European Space Agency (ESA) the number of artificial space debris are in order of 29000 for objects larger than 10cm, 670000 for object larger than 1cm and more than 170 million for sizes larger than 1mm, this is based on scientific model estimations considering that small objects are difficult to be tracked from Earth (ESA,2021). However, the National Aeronautics and Space Administration (NASA) and the United States Department of Defence have successfully catalogued more than 27000 object larger than 10cm in diameter. Due the high impact velocities which can reach 15 km/s all missions in the Low Earth Orbit (LEO) can also be endangered by small sized objects, one the most extended collision happened in 2009 between the active Iridium-33 satellite and the decommissioned Russian Cosmos-2251 satellite which have created a two distinctive debris clouds accounting for more than 2000 large size objects (NASA, 2021). Furthermore, accidental collisions are not the only cause producing space debris, as can be seen in Figure 1, China conducted an anti-satellite test in 2007 on one of its weather satellites of the Fengyun series which created over 2000 debris of various sizes in LEO. The latest intentional collision happened in 2021 when Russia destroyed the Cosmos 1408, no longer operational, generating a cloud of debris with 1500 objects (NASA, 2021).

The oldest artificial space debris in Earth's orbit is the Vanguard-1, the second satellite send to space by the United States in 1958, following the conclusion of its scientific mission in 1964 it remained adrift in orbit. It was predicted that Vanguard-1 would remain in space for 2000 years, however it has been found that solar radiation pressure during high solar activity can reduce its lifetime to about 240 years when it is expected to re-enter into Earth's atmosphere (nssdc.gsfc.nasa.gov).

In 1978, Donald J. Kessler and Burton G. Cour-Palais published the paper *Collision Frequency of Artificial Satellites: The Creation of a Debris Belt*, where the term 'Kessler Syndrome' originated. The results of the paper concluded that if the growth rate of the objects in Earth orbit, catalogued at the time by NORAD would increment, by the beginning of 2000 a population of small space debris can increase dramatically (Donald J. Kessler et. al, 1978). The term has begun to be known to the public thanks to John Gabbard from NORAD when it described in its article the danger of future cascading effect of space debris colliding and the theoretical point where it becomes impossible to launch new missions in orbit. However, over the years the term 'Kessler Syndrome' has begun to be associated, by the press and the general public, to definitions that are distorted by the intended terminology used by John Gabbard in its paper. In 2010 a review of the original article has been published by Donald J. Kessler and Nicholas L. Johnson the definition of this term has been clarified and it concluded that although the term has been exaggerated and distorted from the real intent, the results of the research community in the last 30 years have shown that the future of orbital debris environment will be defined by random collisions (Donald J. Kessler et. al, 2010). On the other hand, thanks to the improvement of mitigation guidelines, adequate collision avoidance capabilities and the latest NASA's LEO-to-GEO Environment Debris model (LEGEND) that can predict future impacts the rate of accidental collisions can be reduce, if 90% of future missions adhere to the current guidelines (NASA, 2021).

In October 1993 the Inter-Agency Space Debris Coordination Committee (IADC) was founded as an international governmental forum intended to exchange information on space debris research activities between member space agencies including the UK Space Agency or the European Space Agency (ESA) (iadc-home.org). The IADC defines space debris as *"Space debris are all man made objects including fragments and elements thereof, in Earth orbit or re-entering the atmosphere, that are non functional"*. It also introduced the concept of 'protected regions' for the LEO and GEO and guidelines on the removal of space debris from these regions, for LEO the main option is de-orbit, by placing the satellite in a lower orbit where atmospheric drag will limit the lifetime after completion of operations, set to 25 years by the IADC. On the other hand, geosynchronous satellites in GEO are required to be removed from the protected region and placed into a higher orbit called super synchronous orbit or disposal orbit where the expected orbital lifetime is of millions of years (International Academy of Astronautics, 2005). The UK published in 2021 for the first time its National Space Strategy where it recognises the growing risk posed by accidental collisions with space debris, furthermore the G7 countries have issued a statement in the summer of 2022 also recognising the expanding hazard of space debris.

However, provided guidelines from the IADC or the European Union Draft Code of Conduct for Outer Space Activities are not yet legally binding under international law, although most national space agencies have been implementing them for years on a voluntary basis. The article 'THE ECONOMICS OF SPACE DEBRIS IN PERSPECTIVE' associates Earth's orbits as a common pool of resources similar to terrestrial natural resources. It states that the overexploitation and pollution of the protected regions by individual users, motivated by short-term gains, can lead to an increase in space debris therefore reducing the value of space activities for the humankind (Marit Undseth, et al. 2020). This implies the urgent need for an international obligation for cooperation for a common interest, similar to the 'Outer Space Treaty' of 1967 UN's General Assembly which states that *'the exploration and use of outer space should be carried out for the benefit and in the interest of all countries, and second, that it should be carried out in due regard of the corresponding interests of all states parties to the Treaty'*. Despite that, some countries such as the United States considers that the vague formulation of Article 1 does not hold any legal responsibilities and cannot be enforced without further clarification (Annette Froehlich, 2019)

1.3 PETER-1 Mission Concept

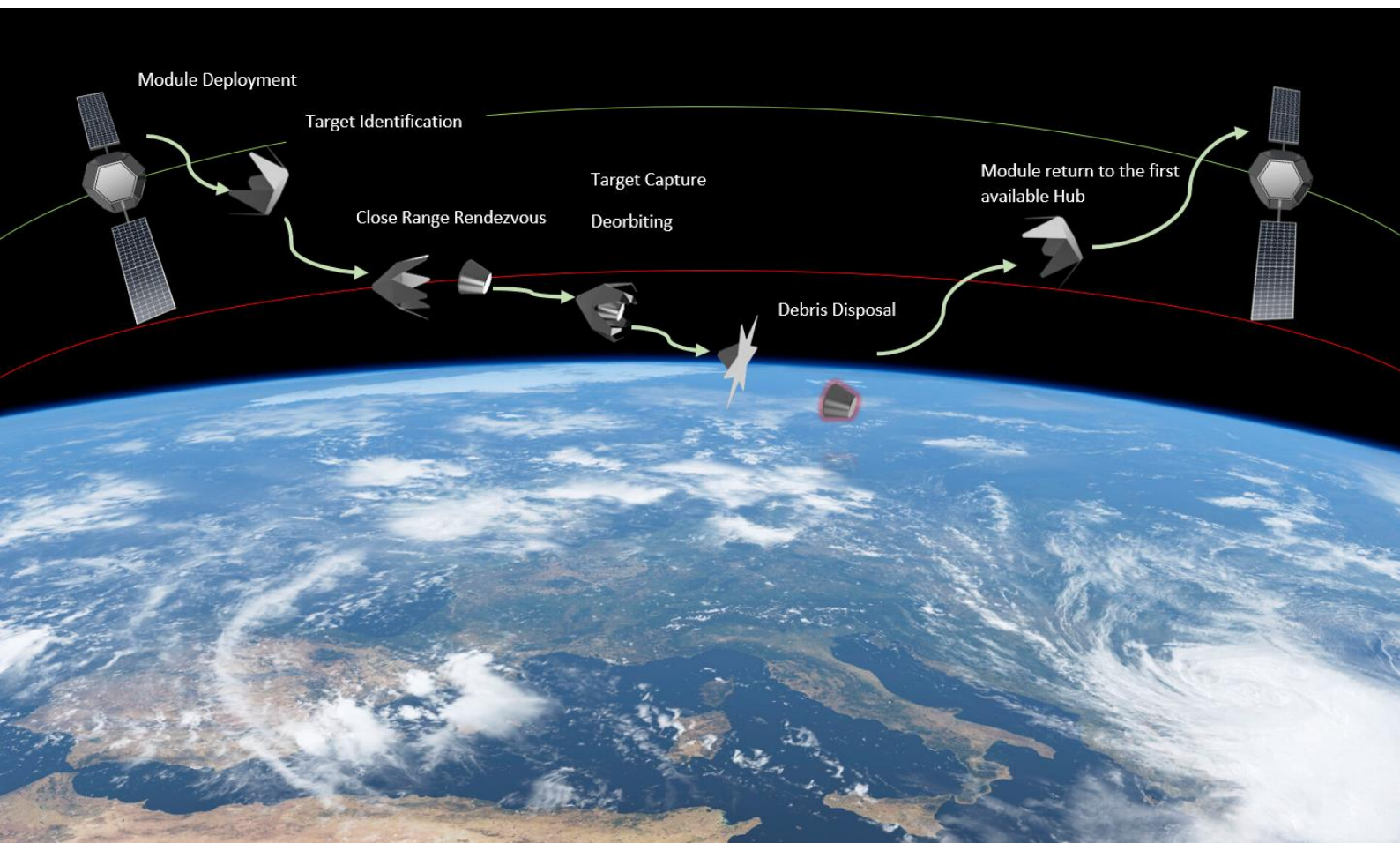


Figure 2 Mission Concept

The report proposes a novel concept for managing space debris by deploying into LEO several station-keeping hubs containing 8 reusable modules that can capture and deorbit space debris of different dimensions. The overall concept of the mission is illustrated in Figure 2, however this is an initial concept that relies on some assumptions such as that the possibility of a module returning to a hub after completing its mission. Some other concepts such as propulsion, orbital mechanics and orbital transfers or standards and requirements for space missions are not within the scope of this report, as this is only an initial proof of concept of a single module covering the overall design and main functionality.

The project aims at developing an autonomous module made out light material and 3D printed components that weighs under 5Kg, the maximum payload for an UR5 robot arm on which the module can be mounted.

Chapter 2: Literature Review

2.1 Mitigation, Remediation and On-Orbit Servicing

As discussed previously the standardisation of mitigation measures across the globe is essential to achieve a safer and cleaner space environment for the humankind. Since 2016 ESA published an annual Space Environment Report and in the latest report from 2022 it has been highlighted that although there has been a gradual increase in the adoption and adherence to space debris mitigation practices, it is crucial to recognize that the implementation of such measures remains inadequate to ensure a sustainable environment in the long term. Moreover, simulated scenarios of long-term evolution of the space environment confirmed what Donald J. Kessler predicted in 1978 as the current changing use of orbits, especially with the introduction of artificial constellations, is leading to a cascade of collision events. Even in the absence of additional launches the current space debris environment is expected to experience further growth due to collisions among existing objects in orbit. It has been speculated that the number of objects bigger than 10cm in LEO would peak to approximately 175000 by 2225 with the current rate of launches and the number of catastrophic collisions will reach 1000 in the same period. This however, are optimistic results as the space debris environment continues to deteriorate and also the technological advancements enable the possibility to send hundreds of satellites at once as part of the artificial constellations. It therefore, accentuates the need for effective space debris mitigation strategies required for managing the end of life of space assets (ESA'S ANNUAL SPACE ENVIRONMENT REPORT, 2022). According to ESA's report the most internationally accepted space debris mitigation measures can be attributed to the following aims:

- The limitation of space debris released during normal operations.
- The minimisation of the potential for on-orbit break-ups.
- Post mission disposal.
- Prevention of on-orbit collisions.

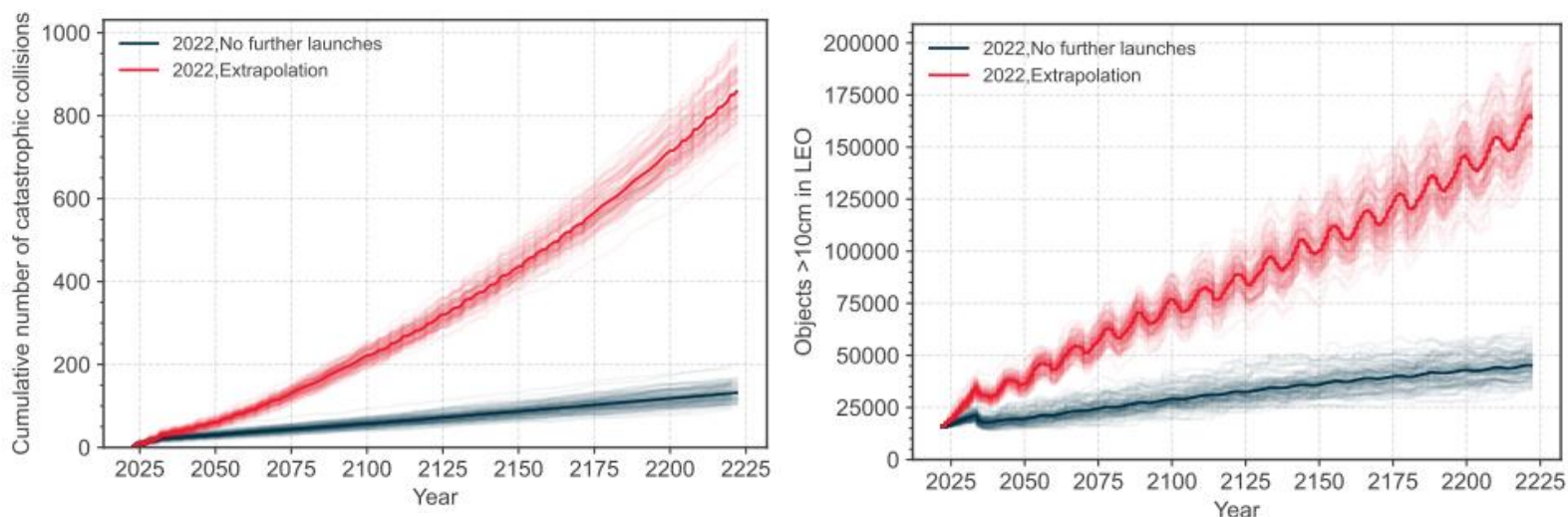


Figure 3: Number of cumulative collisions and number of objects in LEO in the simulated scenarios of long-term evolution of the environment, ESA 2022

Space debris remediation aims to decrease the population of debris by addressing the pre-existing assets already in orbit. This includes the concept of On-Orbit Servicing (OOS) to extend the operational lifetime by sending a spacecraft to perform orbital operations such as satellite repair and refuelling. NASA recognized the importance of OOS missions as early as the 1980s and the most significant example of an OOS mission was the Hubble Space Telescope (HST) Servicing Mission 1 (SM1) in 1993. During this mission astronauts aboard the Space Shuttle Endeavour performed a series of complex tasks to repair and upgrade the HST such as installing the corrective optics to fix the mirror's flaw on board HST. The mission was a success as the HST was designed for OOS and to support periodic servicing by the Space Shuttle thanks to the components on board were engineered to be easily accessible and replaceable by astronauts during servicing missions. Therefore HST is considered to be a 'cooperative object' as it contains proper devices mounted on board to aid autonomous rendezvous and docking/capture operations (RVD). OOS missions can become more complex for satellites that are not equipped with devices suitable for RVD operations, this is the case for most of the older satellites and specially for space debris. This type of objects is called 'uncooperative objects' and the first mission occurred in 1992 with the rescue mission of the Intelsat V1-F3 satellite that required to be re-orbited after a malfunction to its main engine.

Despite the implementation of international agreement and mitigation measures after 1996, the concerning cause for the proliferation of space debris is related to the objects already in orbit. There is a growing support for the implementation of direct retrievals of space debris, in parallel to mitigation measures, that could drastically reduce the number of debris currently in orbit (Livia Savioli, 2015). These missions are known as Active Debris Removal (ADR) and studies have shown that the implementation of such mission are essential to halt the exponential growth predicted of debris collisions in LEO. It has been estimated that in order to stabilize the current situation with space debris, at least five large objects are needed to be removed from orbit every year, this is based on the assumption of a 90% success rate. A lot of research is devoted to the study of different methods for ADR missions such as the use of nets, harpoons, or electrodynamic tethers to capture and deorbit space debris. The University of Surrey led a mission called RemoveDEBRIS which successfully demonstrated different approaches for ADR technology in orbit. The mission launched in 2018, co-founded by the European Commission, to the International Space Station (ISS) where CubeSats have been deployed to act as simulated debris targets. It demonstrated the implementation of different approaches such the use of a net, a harpoon, and a dragsail. Overall, the mission was a success as it demonstrated how this methods could work in a real environment, but more importantly it attracted significant media attention which contributed to raise public awareness to the importance of ADR missions.

One of the most promising techniques for ADR is the use of robotic systems mounted on a 'chaser' to capture, stabilize and deorbit debris objects. ClearSpace-1 is a mission led by the ESA that aims to demonstrate the validity of such systems in ADR for objects of different size and shape. It is scheduled to launch in 2025 when it will attempt remove to the VESPA upper stage located at an altitude of approximately 800km after the launch of VEGA in 2013 (ESA, 2019). The mission phases consist of phasing with the target, far and close range rendezvous, capture and mating operations and finally de-orbiting and controlled re-entry. Very similar to the mission concept presented in this report, although PETER-1 would be required to release the debris into the atmosphere and return to the orbital plane of the first available hub, making it reusable and not destroyed in the atmosphere.

2.2 Computer Vision and Deep Learning

Computer Vision (CV) research started in 1970s by the early pioneers of artificial intelligence and robotics at institutions such as MIT or Stanford. It focuses on enabling machines to interpret, analyse and extract meaningful features and patterns from visual information such as images and videos. Early research in this field began with the ambitious agenda of researchers to create the perception component and to mimic the human cognition, with the ultimate goal of endowing robots with intelligent behaviour. However, researchers quickly realized that the task of creating machines that can recover the three-dimensional structure of the world was much more complex than they initially anticipated. This made CV distinct from existing fields, such as digital image processing, and enable the ongoing development of novel algorithms and techniques to enable machines to extract meaning from visual data (Richard Szeliski, 2022).

The emergence of deep learning and artificial neural networks (ANN) in recent years led to significant improvements in Computer Vision, particularly in areas such as image recognition, object detection and segmentation or other AI studies of computer vision. Deep learning is a powerful form of machine learning that draws upon insights from neuroscience, statistics and applied mathematics to create networks that can learn from data in a way that resembles the human brain. Deep neural networks are distinguished from other machine learning models by their ability to solve complex nonlinear problems and extract high-level features from input data by using multiple layers of artificial neurons. This fundamental deep network is called multi-layer perceptron (MLP) and is a mathematical function that maps a set of input values to output values, consisting of multiple layers of interconnected artificial neurons.

The process of learning in a neural network can be expressed as finding the optimal set of weights and biases that are used to compute the output of each layer. In order to obtain the optimal weights, the algorithm repeatedly updates them by minimizing the loss defined by the model. The training procedure consists of a loop that is repeated for a fixed number of iterations, defined by epochs and sample size. First, a mini-batch of training samples is fed into the first layer of the network and then transformed into high-level features by multiplying the weights and applying an activation function at each layer. Next, the mean loss is calculated using the true and estimated values of the output for each mini-batch. The gradient of the loss is then calculated with respect to each weight, as the signal is propagated back from the output layer to the input layer. The weights are updated in the direction of decreasing loss using an optimization algorithm, such as the stochastic gradient descent (Richard Szeliski, 2022).

In 1943, Warren McCulloch, an American neurophysiologist and cybernetician at the University of Illinois at Chicago, and Walter Pitts, a self-taught logician and cognitive psychologist published 'A Logical Calculus of the ideas Imminent in Nervous Activity'. They introduced the first mathematical model of an ANN which is known as the 'McCulloch-Pitts neuron'. In the early stages MLPs were a powerful tool for solving complex nonlinear problem, however they had certain limitations in handling high-dimensional data such as images. In the early 1990s, Yann LeCun and his team introduced a new type of neural network architecture called Convolutional Neural Network (CNN), specifically designed to address this limitation. They developed a CNN called LeNet-5, based on the notion of using convolutional layers to extract features from images which later began to be used by banks to recognize hand-written cheques (Hagyeong Lee et. al, 2019).

2.2.1 Stereo Vision and Depth Estimation

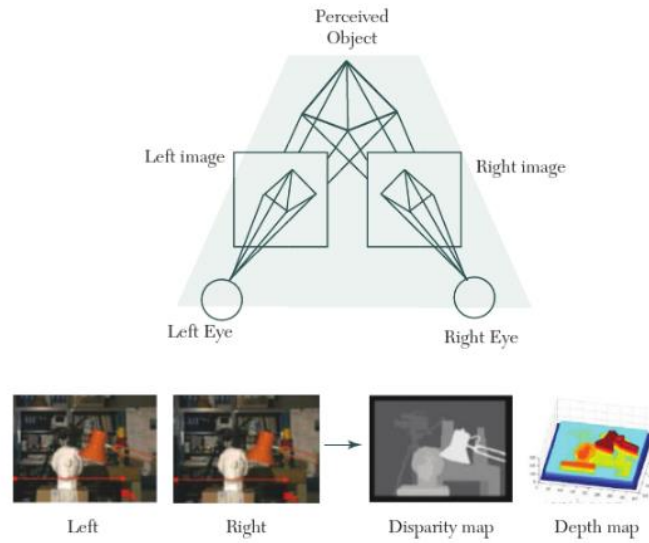


Figure 4 Stereo vision

Stereo Vision is the process of extracting three-dimensional information from multiple two-dimensional views of a scene (S. R. Vijayalakshmi et. al, 2019). The goal of this method is to extract depth information from two or more cameras by comparing their respective images and creating correspondence maps across the images taken of the same scene (Jaehoon Cho et. al, 2019) (Figure 4). Given a pixel in one image, representing a point in real world, the correspondence of the pixel in another image can be found using the concept of epipolar geometry. It may appear that finding corresponding points would require a comprehensive search across the entire images, but the epipolar constraint limits the search to single line called the epipolar line (inf.ed.ac.uk, 1997). For instance Figure 5 shows how a pixel in one image with the camera centre at c_0 is projected onto an epipolar line segment in the second image with the camera centre at c_1 . The line segment is limited at one end by the projection of the original viewing ray at infinity, and the other end by the projection of c_0 into the second camera at e_1 . This is known as epipole, which is defined as the point of intersection of the line joining the camera centres, also called the baseline, with the image plane (Richard Hartley, 2004). If the epipolar line l_1 from the second image is projected back into the first, it results in another segment bounded by the other epipole e_0 . By extending both segments to infinity, produces a pair of corresponding epipolar lines which represent the intersection of the two image planes with the epipolar plane passing trough c_0 and c_1 as wells as the point of interest p (Richard Szeliski, 2022).

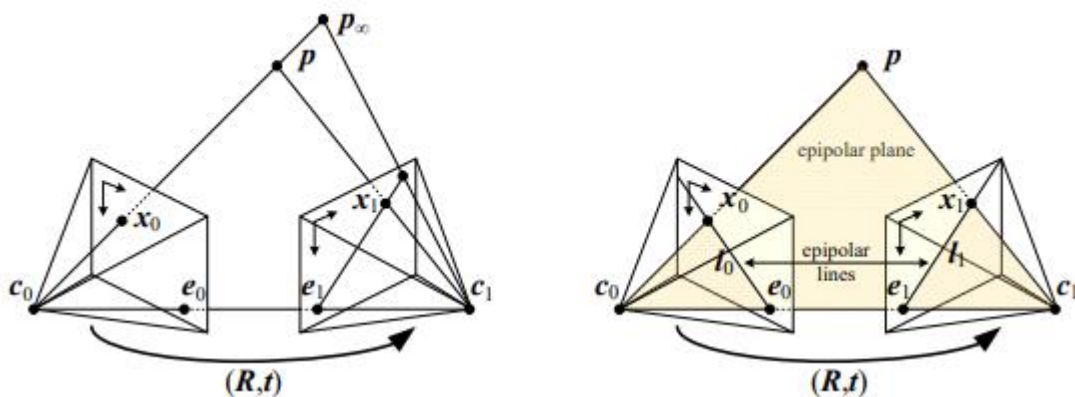


Figure 5 Epipolar Geometry

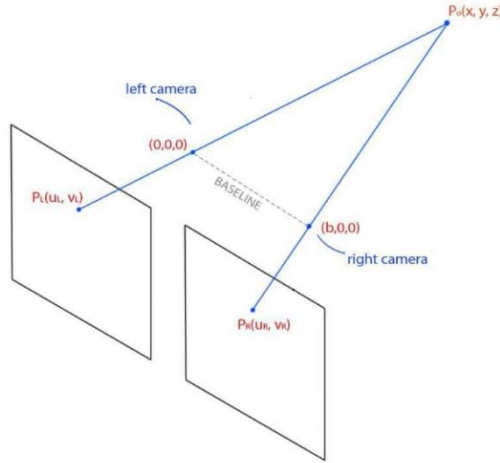


Figure 6 Image formation using a stereo camera

Considering $P_0(x, y, z)$ as the position of the point of interest the real world coordinates and $P_L(u_L, v_L)$ the position in the left camera as well as $P_R(u_R, v_R)$ in the right camera respectively in the image plane coordinates. The perspective projection equations for a calibrated system (the intrinsic and extrinsic parameters of the two cameras are known) can be written as follows:

$$u_L = f_x \frac{x}{z} + O_x$$

$$u_R = f_x \frac{x - b}{z} + O_x$$

$$v_L = f_y \frac{y}{z} + O_y$$

$$v_R = f_y \frac{y}{z} + O_y$$

Where,

f_x, f_y is the focal length of the camera along x and y axis

u, v are the coordinates of the point in the image plane, in pixels

O_x, O_y is the optical centre of the camera, in pixels

b is the line between the centres of the cameras, also called baseline

Solving the projection equations, the coordinates x, y, z (where z is the depth of the point from the camera) of the point of interest P_0 can be found solving the following equations.

(learnopencv.com, 2021).



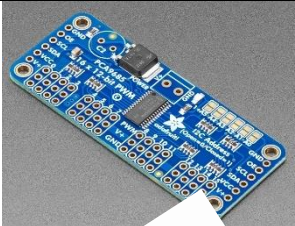

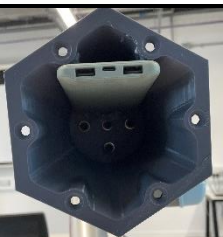
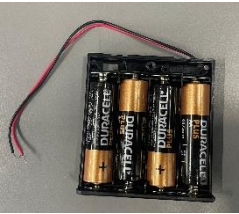
$$x = \frac{b(u_L - O_x)}{u_L - u_R}$$



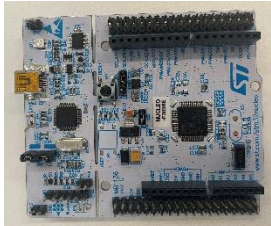



$$y = \frac{bf_x(v_L - O_y)}{f_y(v_L - u_R)}$$

$$z = \frac{bf_x}{u_L - u_R}$$

Chapter 3: Methodology

3.1 System Components

Name	Reference Image	Description	Implementation
DS3218 Servo Motor		<ul style="list-style-type: none"> -Operating Voltage: 4.8 ~ 6.8V -Weight: 60 g -Operating frequency: 50-330Hz -Gear ratio: 275 -Idle current: 4mA -Pulse width range: 500~2500μs -Operating travel: 270° (PWM 500-2500μs) 	<ul style="list-style-type: none"> -Control the six arms of the module -Connected to the shaft using a 5mm inner diameter Gear Synchronous Timing Pulley and Belt
SG90 Servo Motor		<ul style="list-style-type: none"> -Operating Voltage: 4.8 ~ 6V -Weight: 14.7 g -Pulse width range: 100~2000μs -Operating travel: 180° (PWM 100-2000μs) 	<ul style="list-style-type: none"> -Connect to the two segments of the arm -Control the upper segment
PCA9685 16-Channel Servo Driver		<ul style="list-style-type: none"> -Operating power supply voltage range: 2.3 ~ 5.5V -I²C-bus controlled -12-bit PWM (4096 steps) 	-Connect the six SG90 motors to the STM32F303RE microcontroller using I ² C
HC-05 Bluetooth Module		<ul style="list-style-type: none"> -Operating Voltage: 4V to 6V -Operating Current: 30mA -Range: <100m -USART Serial Communication -Supported baud rate: 9600,19200,38400,57600, 115200,230400,460800. 	<ul style="list-style-type: none"> -Receive data from the Raspberry Pi4 and -Send data to STM32F303RE
HG05636A Power Bank		<ul style="list-style-type: none"> -Capacity: 10000mAh 37Wh -1 Type C Port -2 Type A Port -Voltage Output 5V -Current Output 3A (Type C Port) -Current Output 2.1A (Type C Port) 	-Supply power to the Raspberry Pi4, the STM32F303RE and the OAK-D Lite camera
Generic battery holder 4xAA Batteries		<ul style="list-style-type: none"> -Nominal Voltage: 1.5V -Weight: 24g 	-Supply 6V of power to the PCA9685

Name	Reference Image	Description	Implementation
OAK-D Lite Camera		<ul style="list-style-type: none"> -Sensor Colour Camera: IMX214 -Sensor Stereo pair: OV7251 -Resolution Colour Camera: 13MP -Resolution Stereo pair: 480P -Max Framerate Colour Camera: 35FPS -Max Framerate Stereo pair: 120FPS -Robotics Vision Core 2 (RVC2) processor 	-Send RGB-D video stream to the Raspberry Pi4
HC-SR04 Ultrasonic Sensor		<ul style="list-style-type: none"> -Operating Voltage: 5V -Operating Current: 15mA -Operating Frequency: 40Hz -Range: 2cm to 4m 	-Send distance measurement to the Raspberry Pi4
STM32F303RE Microcontroller		<ul style="list-style-type: none"> - Processor ARM Cortex-M4 32-bit CPU -Voltage range: 2 to 3.6V - 512 Kbytes of Flash memory - 64 Kbytes of SRAM - GPIO: 115 I/O -USB 2.0 	-Receive data from the HC-05 to control the servo motors
Raspberry Pi4		<ul style="list-style-type: none"> -Processor: Broadcom BCM2711, quad-core Cortex-A72 (ARM v8) 64-bit SoC @ 1.5GHz -Memory: 4GB LPDDR4 -Connectivity: 2.4 GHz and 5.0 GHz wireless LAN, Bluetooth 5.0, BLE Gigabit Ethernet -2 x USB 3.0 ports -2 x USB 2.0 ports. -GPIO: Standard 40-pin GPIO header 	<ul style="list-style-type: none"> -Receiving video stream from the OAK-D Lite and the x y z coordinates of the object. -Receiving distance measurement using the HC-SR04 -Sending commands to the HC-05
Sourcing Map 5mm Inner Diameter Rotatable Universal Joints		<ul style="list-style-type: none"> -2 Universal Joints connected with 10mm aluminium pin. -6 joints in total 	Although it has been attempted to connect the shafts using a single Universal Joint, but it was found that it would prohibit the arms to move in synchronous. Connecting two joints allows the arms to move in synchronous with an equal torque distributed around the six shafts
Sourcing Map Deep Groove Ball Bearings 5mm		<ul style="list-style-type: none"> -Inner Diameter: 5mm -Outer Diameter: 16mm -Thickness: 5mm 	- A total of 12 bearing has been used, 2 per each body component on the hinge mechanism

3.2 System Implementation Diagram

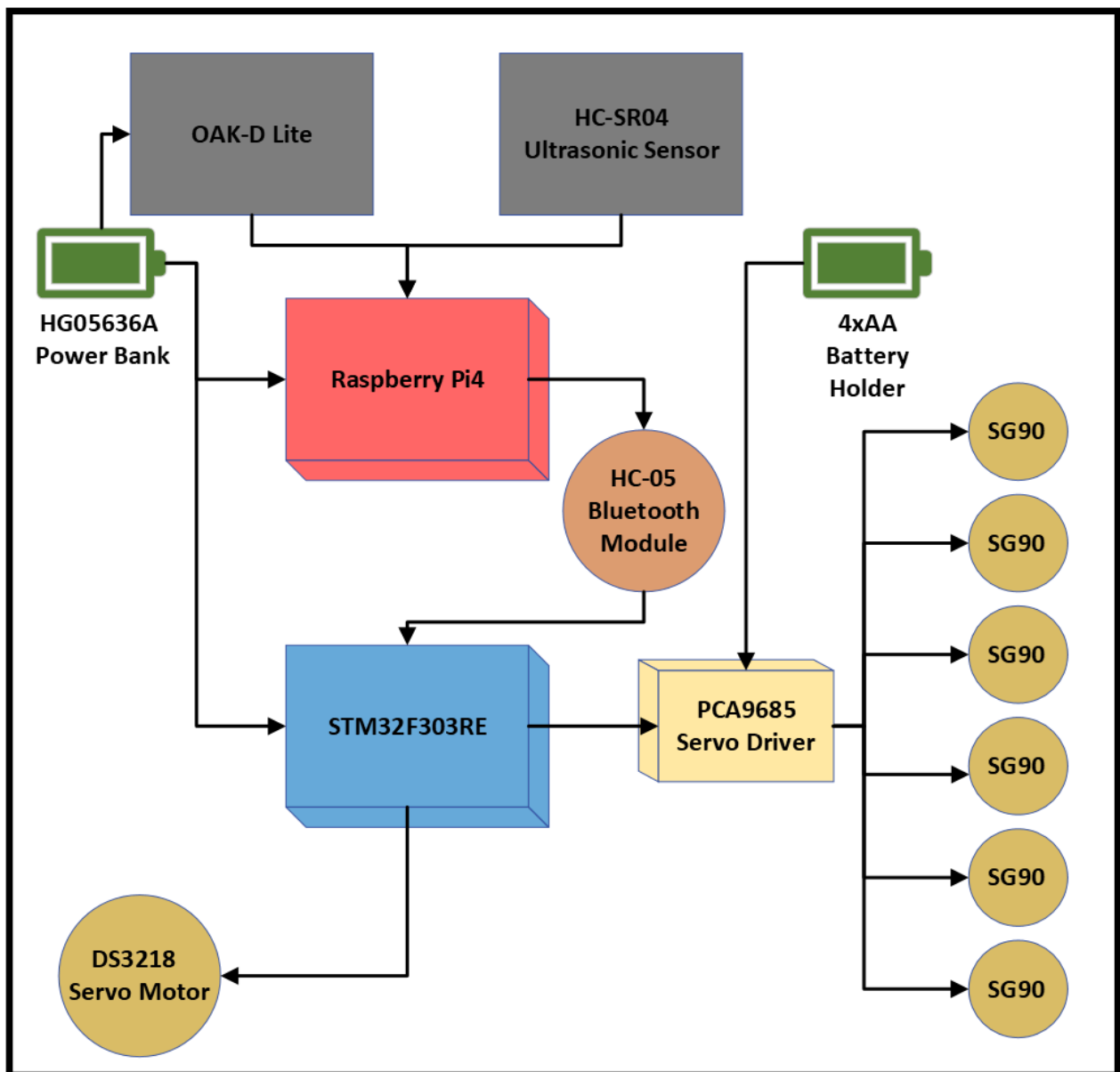


Figure 7 System Implementation

3.3 Object Detection

One key challenge in performing active space debris removal is identifying and tracking the debris objects. In order to achieve effective and efficient debris removal on object that can vary in size, shape and reflectibility, a reliable and robust object detection algorithm is necessary to identify and track the debris objects in real-time. Convolutional Neural Networks (CNN), a type of Deep Learning algorithm, have demonstrated remarkable performance in the field of object detection. The YOLO (You Only Look Once) algorithm is considered the most effective object detector CNN to date, due to its high real-time performance and high accuracy especially on embedded devices (Wei Fang et. al,2019). The algorithm was first introduced in by Joseph Redmon, Santosh Divvala, Ross Girshick and Ali Farhadi in 2015, which revolutionized the field of object detection by providing a faster and more accurate method than traditional methods. The YOLO framework consists of three main components: Backbone, Neck and Head. The Backbone encodes the image fed into the input layer and extracts features that are sent to the Head through the Neck which creates feature pyramids based on the extracted features. The Head contains the output layers that produce model predictions (learnopencv.com, 2022). Compared to other conventional object detectors, YOLO is defined as a Single-Stage Detector (SSD) which means that the algorithm is performing object detection on the entire image in a single pass and it outputs the class probabilities and the bounding box coordinates. This is considered to be faster than Multiple-Stage Detector (MSD) which processes the image in multiple stages. An MSD algorithm generates a set of candidate regions of interest (ROI), using a Region Proposal Network (RPN), which then are pooled and classified to obtain the final detection results. In SSD the detection head is applied directly on to the feature map, while on the MSD approach the RPN is applied to the feature map which subsequently produces the results as it can be seen in Figure 8. Although MSDs models are considered to be more accurate, they require more computational resources and are slower compared to SSD detectors (pyimagesearch.com, 2022).

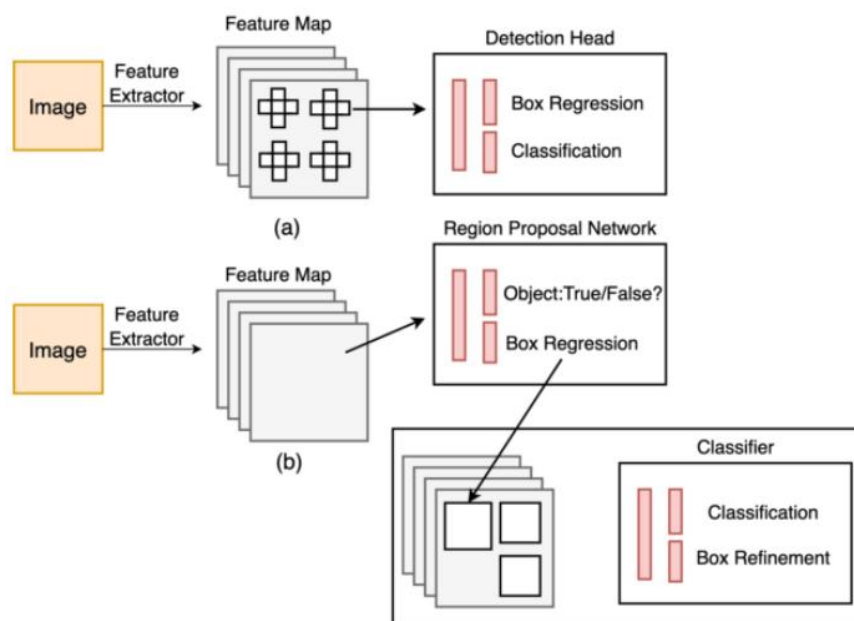


Figure 8 Comparison between SSD and MSD models

3.3.1 Dataset Preparation and Training

For the project it has been decided that the most suitable model to use is the YOLOv7-tiny as is the latest version of the 'tiny' models from the YOLO family. This version is optimized for embedded devices with limited computational resources as it uses 6.2 million parameters compared to 36.9 million in the YOLOv7 version. The YOLOv7-tiny model achieved a validation Average Precision (AP) (metric used to evaluate the accuracy of object detection models) of 35.2% on the COCO dataset, compared to 51.2% on the full version. This is resulting in the smaller version to be less accurate, yet remains the most efficient model for embedded devices (<https://learnopencv.com>, 2022).

The object to be used during simulations has been made using two blocks of Extruded Polystyrene (XPS) foam board which have been sculpted, using a hot wire sculpture, and painted to resemble a space debris (Figure 9).

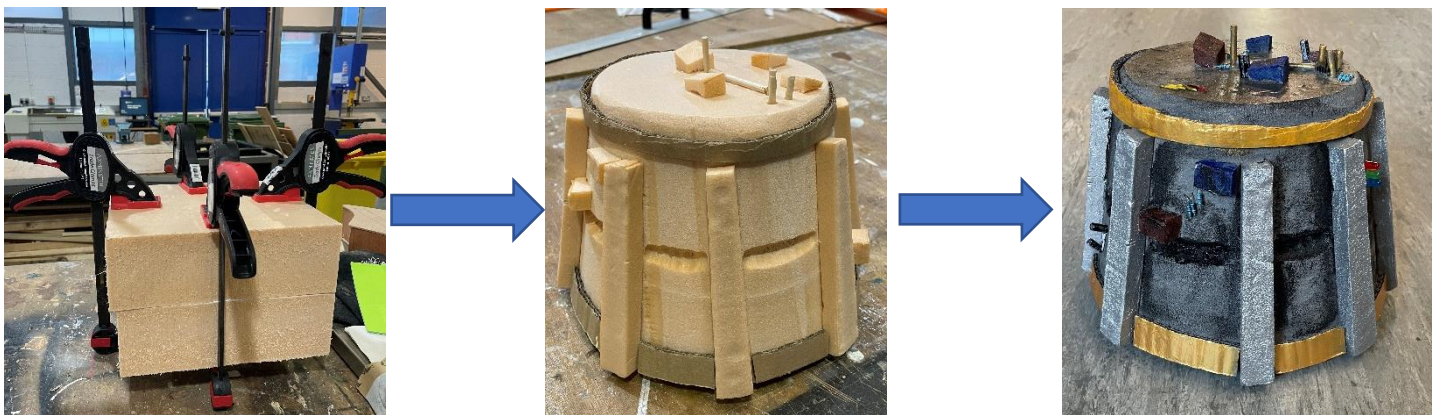


Figure 9 Simulated Space Debris Object

The dataset consists of 150 images of the object which have been labelled using the YOLO format (example in Figure 10) and resized to 640x640, using the Roboflow online platform at <https://roboflow.com/>. Moreover, in order to expand the dataset and increase diversity in the data, it has been used data augmentation by applying image rotation and increased brightness, resulting in the dataset to be a total of 400 images (Figure 11). The dataset has been divided into 70% training data, 20% test data and 10% validation data.

```
[object-class-id] [center-x] [center-y] [width] [height]
0 0.300926 0.617063 0.601852 0.765873
```

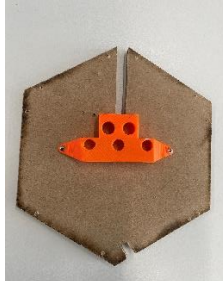

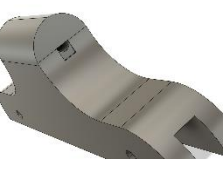
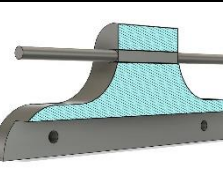

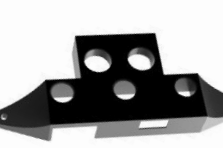
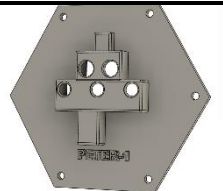
Figure 10 YOLO label format

The model has been trained using the 'YoloV7_training.ipynb' tutorial on GoogleColab provided by Luxonis. The training process involved 400 epochs, a batch size of 32 and the image size set to 640x640.



Figure 11 Labelled Dataset

3.4 Design Evolution and Manufacturing

Name	Reference Image	Description	Material and Components	Manufacturing Process	Mass	Pass / Fail	Comments
Base		Hexagonal shaped board. The six arms are connected to it together with the front plate and the body of the Module.	Medium Density Fibreboard (MDF)	Laser cutting.	380g	PASS	The component meets the manufacturing criteria as it is robust and can be easily manufactured.
Hinge v_1		The initial design for the hinge mechanism. It is composed by a fixed component (connected to the base) and a moving component (connected to the arm)	-PLA - One 5-mm diameter circular aluminium shaft. -Three bearings with 5 mm inner diameter	3D Printing	Arm component 18g Body component 20g	Fail	The shaft requires to be under an interference fit with the arm component. Because the component is 3d printed, it allows the slot for the shaft to expand therefore eliminating the force fit
Hinge v_2		The arm component has been modified to allow the insertion of 'D' shaped shaft	PLA	3D Printing	41g	Fail	The non-circular cross-section of the 'D' shaft caused the arm component to no longer be concentric with the bearings. Resulting in the misalignment of the two components
Hinge v_3		Because of the flaw in the previous designs, it has been adopted a square cross-section for the shaft slot	PLA	3D Printing	40g	Pass	The square cross-section allows a custom shaft to be inserted under interference fit and remain concentric with the bearings. The custom shaft has circular extremities to be inserted in the bearings, and a centred square section
Hinge v_4		The base component has been re-designed to include only two bearings. The lower part consists of two edges of 45° instead of 90° as the initial design	PLA	3D Printing	Arm component 40g Body component 34g	Pass	The fourth version has been chosen as the final design of the hinge mechanism
Case		Initial design for the case of the OAK-D Lite camera and the ultrasound sensor	PLA	3D Printing	28g	Fail	The part is functional, but it has been decided to design a case that will merge into a front panel for aesthetic reasons
Front Panel		The front panel combined with the case and the name of the project	PLA	3D Printing	139g	Pass	It includes 5 holes for the bolts required for the final assembly

Name	Reference Image	Description	Material and Components	Manufacturing Process	Mass	Pass / Fail	Comments
Body v_1		The initial design of the body connects the upper part and the lower part using six segments	N/A	N/A	N/A	Fail	The part has not been manufactured but only 3D modelled. This is due to the high probability of the segments breaking under shear force
Body v_2		The body consists of two separate parts which can be joined by means of bolts with a length of 10 mm. The opening on the lower section is essential to accommodate the servo motor connected to the shaft	PLA	3D Printing	564g	Pass	The upper component is connected to the UR5 Robot Arm and it contains the power bank to power the STM32F303 and the Raspberry Pi 4. The lower component contains the following: -STM32F303 -PCA9685 servo controller -BT-05 Bluetooth module -Battery holder for 4 AA batteries
UR5 Mount		UR5 component: -four 15mm deep holes to connect to the UR5 -five 20mm deep holes to connect to the module component -one pin hole Module component: -five 10mm deep hole to connect to the UR5 component	Aluminium	CNC	368g	Pass	Due to the limited depth of the four mounting holes on the UR5 Robot Arm, which are only 5 mm, it has been determined that a custom mounting solution is required to securely hold the module in place
Module Arm v_1		The module arm is divided into a lower part connected to the body and an upper part	Medium Density Fibreboard MDF	Laser Cutting	214g	Fail	The servo motor was not capable of lifting the arm due to the significant mass of the arm
Module Arm v_1		Same design as previous version	Extruded Polystyrene XPS	Bandsaw	13g	Pass	As a result of the lower mass the motor can control the arm as expected
Upper hinge v_1		Hinge mechanism to connect the lower part to the upper part of each arm. It also contains an enclosure for an SG90 Micro Servo Motor	PLA	3D Printing	64g	Fail	Due to its mass the main servo motor was unable to lift the arms
Upper hinge v_2		An off the shelf drawn butt hinge connect using cable to the arm.	Brass	Off the shelf component	16g	Fail	Although the mass is significantly lower than the previous version the main servo motor remains incapable of lifting all six arms simultaneously

Chapter 4: Testing and Results

4.1 YOLO Model Results

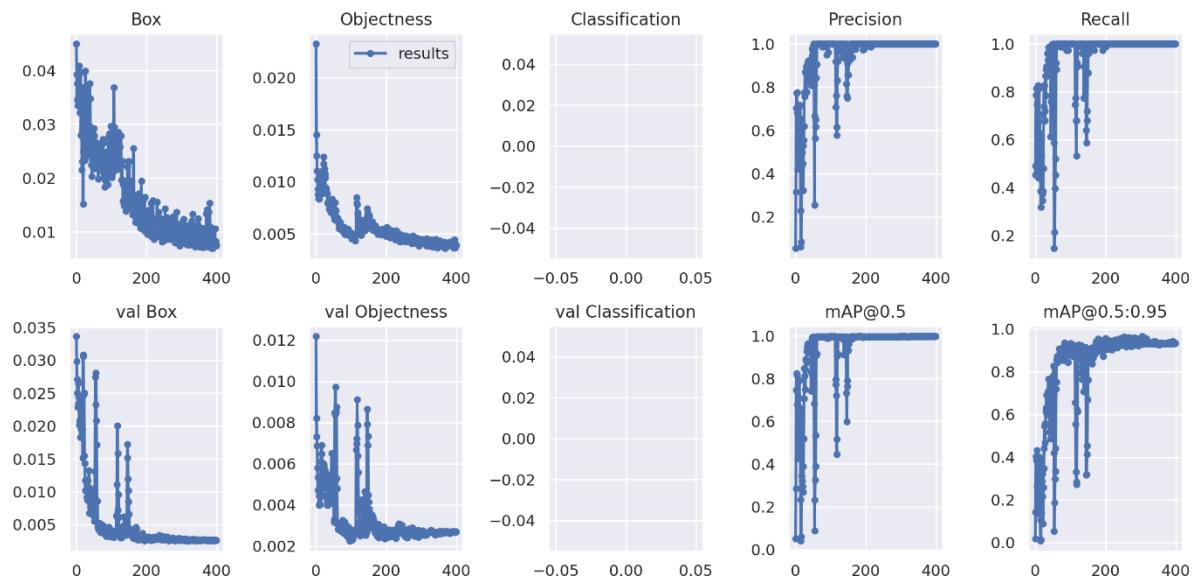


Figure 12 Results from the YOLO training on GoogleColab

The model was trained using Transfer Learning, meaning that it used a pre-trained model of the YOLOv7 trained on the COCO dataset with over 330000 images. Despite multiple iterations, the model failed to perform as expected as a consequence of the images in the dataset being labelled and resized incorrectly. However, after the dataset has been reviewed and relabelled the performance increased drastically. To determine if the model is performing well there are some metrics that can be analysed such as the loss function, precision, and recall.

Figure 12 illustrates the results of the best performing iteration on 400 epochs with a dataset of 400 images. The 'Box' represents the loss function of the prediction box and it refers to the accuracy of the bounding boxes generated by the model. The aim is that the bounding boxes are as close as possible to the object and a smaller value represent a smaller difference between the contours of the object and the bounding box. The model performed well reaching a value of 0.005 during training and 0.001 during validation, however this could have been improved by refining the labels on the images. Objectness loss indicates the error is the probability that an object exists within a bounding box, smaller the value represents a more accurate detection. During training the Objectness value reached 0.0008, however during validation it started to increase after 200 epochs.

Precision measures the proportion of true positive among all positive predictions, for instance if the model identifies 50 cars and in the image there are 100 cars, the precision is 50%. On the contrary recall estimates the model accuracy to label all positive objects in the image. For example, if a model detects 100 cars and 70 are correct, the recall is 70%. In the model the values for precision and recall reach 100% at approximately 200 epochs. Similarly, the mAP (medium Average Precision) value for IoU (Intersection over Union) at 0.5 shows a peak value of 1 at around 200 epochs.

4.2 Module implementation

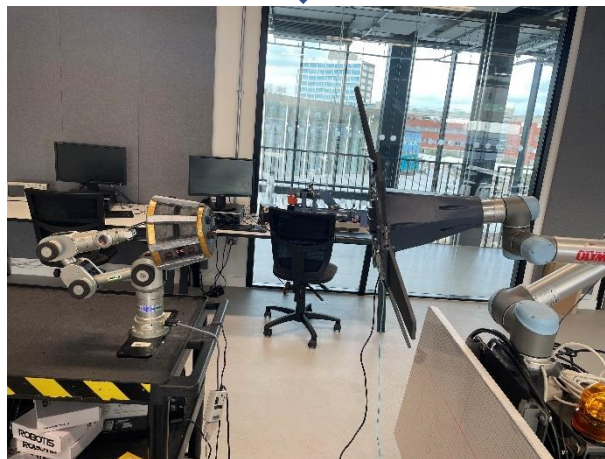


Figure 13 Module Simulation

The simulation has been performed in the laboratory by mounting the module on the UR5 robot arm and the simulated space debris on Katana robot arm. The system performed relatively as expected although the upper section of the arms has not been implemented as the total mass would prevent the arms to move. This was caused by the belt slipping on the on the main motor, despite it has been attempted to introduce a belt tensioner (Figure14) the belt continued to skid. Therefore, the final implementation of the system is at follows:

1. The distance from the object is calculated using the depth estimation function implemented using Python on the Raspberry Pi4. The data is received from the OAK-D camera stereo vision.
2. If the distance is above 2.5m (Figure 15) the arms remain in the 'IDLE' position. The DS3218 servo motor is set at 25°
3. If the distance is between 0.5cm and 2.5m (Figure 15) the Raspberry Pi4 sends the character '1' to the STM32F303RE using the HC-05 Bluetooth module
4. The STM32F303RE receives the character '1' and moves the arms using the DS3218 servo motor to the 'READY' position, at an angle of 135°
5. The minimum range of the OAK-D camera is approximately 35cm, caused by disparity in the stereo cameras. Therefore, for distances smaller than 50cm the distance to the objected is calculated using the HC-SR04 Ultrasonic Sensor.
6. The arms will move to position 'CLOSED' when the distance measured is smaller than 50cm.
7. If the object is not longer detected the arms will move back to the 'IDLE' position.



Figure 14 Belt Tensioner

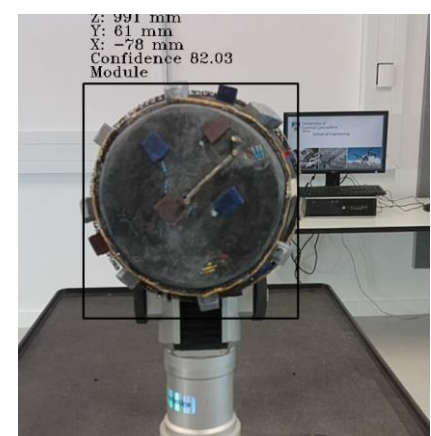
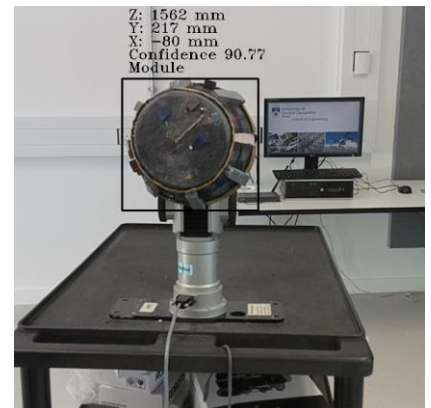


Figure 15 Object detected using the OAK-D camera

Chapter 5: Conclusion and further development

The proof of concept developed and described within this report illustrated the ability of detecting and capturing an object using a pretrained model using the YOLO object detection algorithm. The research was driven by the need of developing new system to perform active space debris removal. Although the prototype is currently in its early stages, it has the potential to be further developed into a fully functional system.

The YOLO model could be improved by adding more images to the dataset which currently only contains 150 original images plus 250 augmented images. A robust dataset requires at least 1000 images which can then be further augmented. Furthermore, the mechanical system must be changed to sustain a higher payload and prevent belt slippage.

References

- Types of orbits* 2020,
Available: https://www.esa.int/Enabling_Support/Space_Transportation/Types_of_orbits.
- ESA commissions world's first space debris removal* 2019
Available: https://www.esa.int/Space_Safety/Clean_Space/ESA_commissions_world_s_first_space_debris_removal.
- "Position Paper on Space Debris Mitigation, Implementing Zero Debris Creation Zones", 2005
- Epipolar geometry*, .
Available: https://homepages.inf.ed.ac.uk/rbf/CVonline/LOCAL_COPIES/OWENS/LECT10/node3.html.
- Inter-Agency Space Debris Coordination Committee*, . Available: https://www.iadc-home.org/what_iadc.
- LEGEND : 3D/OD Evolutionary Model*, .
Available: <https://orbitaldebris.jsc.nasa.gov/modeling/legend.html>.
- Vanguard 1d*, . Available: <https://nssdc.gsfc.nasa.gov/nmc/spacecraft/display.action?id=1958-002B>.
- Aditya Sharma 2022, , *Understanding a Real-Time Object Detection Network: You Only Look Once (YOLOv1)*.
- Annette Froehlich 2019, *Space Security and Legal Aspects of Active Debris Removal*
- Constance McLaughlin Green and Milton Lomask 1970, "Vanguard: A History"
- DONALD J. KESSLER AND BURTON G. COUR-PALAIS 1978, "Collision Frequency of Artificial Satellites' The Creation of a Debris Bel"
- ESA Space Debris Office 2022, *ESA'S ANNUAL SPACE ENVIRONMENT REPORT*.
- Hagyeong Lee, J.S. 2019, "Introduction to convolutional neural network using Keras; an understanding from a statistician"
- Jaehoon Cho, Dongbo Min, Youngjung Kim, , Kwanghoon Sohn 2019, "Deep Monocular Depth Estimation Leveraging a Large-scale Outdoor Stereo Dataset"
- Kukil, S.R. 2022, , *YOLOv7 Object Detection Paper Explanation & Inference*.
Available: <https://learnopencv.com/yolov7-object-detection-paper-explanation-and-inference/#:~:text=The%20YOLOv7%20model%20can%20detect,people%20who%20are%20far%20away>.
- Livia Savioli 2015, *ANALYSIS OF INNOVATIVE SCENARIOS AND KEY TECHNOLOGIES TO PERFORM ACTIVE DEBRIS REMOVAL WITH SATELLITE MODULES*, Università degli Studi di Padova.
- Marit Undseth, Claire Jolly , Mattia Olivari 2020, "THE ECONOMICS OF SPACE DEBRIS IN PERSPECTIVE"
- Mark Garcia 2021, , *Space Debris and Human Spacecraft*.
Available: https://www.nasa.gov/mission_pages/station/news/orbital_debris.html.

Richard Hartley 2004, *Multiple View Geometry in Computer Vision*

Richard Szeliski 2022, *Computer Vision Algorithms and Applications*

S. R. Vijayalakshmi, S.M. 2019, *Embedded Vision An Introduction*

Satya Mallick, K. 2021, , *Stereo Vision and Depth Estimation using OpenCV AI Kit.*

Available: <https://learnopencv.com/stereo-vision-and-depth-estimation-using-opencv-ai-kit/>.

Wei Fang, Lin Wang & Peiming Ren 2019, "Tinier-YOLO: A Real-Time Object Detection Method for Constrained Environments"

Bibliography

Pose determination of passively cooperative spacecraft in close proximity using a monocular camera and AruCo markers _ Elsevier Enhanced Reader b, .

Aglietti, G.S., Taylor, B., Fellowes, S., Salmon, T., Retat, I., Hall, A., Chabot, T., Pisseloup, A., Cox, C., Zarkesh, A., Mafficini, A., Vinkoff, N., Bashford, K., Bernal, C., Chaumette, F., Pollini, A. & Steyn, W.H. 2020, "The active space debris removal mission RemoveDebris. Part 2: In orbit operations", *Acta astronautica*, vol. 168, pp. 310-322.

Biesbroek, R., Soares, T., Hüsing, J. & Innocenti, L. *THE E.DEORBIT CDF STUDY: A DESIGN STUDY FOR THE SAFE REMOVAL OF A LARGE SPACE DEBRIS.*

Castronuovo, M.M. 2011, "Active space debris removal—A preliminary mission analysis and design", *Acta astronautica*, vol. 69, no. 9, pp. 848-859.

Faure, M., Henry, D., Cieslak, J., Colmenarejo, P. & Ankersen, F. Apr 20, 2022, "A Hoo control solution for space debris removal missions using robotic arms: the ESA e.Deorbit case", IEEE, Piscataway, pp. 122.

Flores-Abad, A., Ma, O., Pham, K. & Ulrich, S. 2014, "A review of space robotics technologies for on-orbit servicing", *Progress in aerospace sciences*, vol. 68, pp. 1-26.

Forshaw, J.L., Aglietti, G.S., Fellowes, S., Salmon, T., Retat, I., Hall, A., Chabot, T., Pisseloup, A., Tye, D., Bernal, C., Chaumette, F., Pollini, A. & Steyn, W.H. 2020, "The active space debris removal mission RemoveDebris. Part 1: From concept to launch", *Acta astronautica*, vol. 168, pp. 293-309.

Kessler, D.J., Johnson, N.L., Liou, J.-. & Matney, M. *The Kessler Syndrome: Implications to Future Space operations Retired NASA, 2 NASA.*

Lange, M., , , , Pegg ; Dirk Jacobsen ; Tom Debraekeleer ; Roberto Lampariello, Katherine, , ;. & Canetri ; John Ratti, M. *Martijn Theybers (2)*, Andrew Wolahan.

Ledkov, A. & Aslanov, V. 2022, "Review of contact and contactless active space debris removal approaches", *Progress in aerospace sciences*, vol. 134, pp. 100858.

Liu, E., Yan, Y. & Yang, Y. 2021, "Analysis and determination of capture area for space debris removal based on reachable domain", *Advances in space research*, vol. 68, no. 3, pp. 1613-1626.

Wormnes, K., Le Letty, R., Summerer, L., Schonenborg, R., Dubois-Matra, O., Luraschi, E., Cropp, A., Krag, H. & Delaval, J. *ESA TECHNOLOGIES FOR SPACE DEBRIS REMEDIATION.*

Zhao, P., Liu, J. & Wu, C. 2020, "Survey on research and development of on-orbit active debris removal methods", *Science China. Technological sciences*, vol. 63, no. 11, pp. 2188-2210.

IADC Report on the Status of the Space Debris Environment Issued by IADC Working Group 2 / Steering Group Internal Task 39.2 Issue 1 Revision 0 2023, .

IADC Statement on Active Debris Removal Issued by IADC Steering Group 2022, .

IADC Space Debris Mitigation Guidelines Issued by IADC Steering Group and Working Group 4 2020, .

Bernhard, P., Deschamps, M. & Zaccour, G. 2023, "Large satellite constellations and space debris: Exploratory analysis of strategic management of the space commons", *European journal of operational research*, vol. 304, no. 3, pp. 1140-1157.